

Common Envelope Evolution

Robert Wissing

Lund Observatory
Lund University



2016-EXA100

Degree project of 15 higher education credits
January 2016

Supervisor: Ross Church

Lund Observatory
Box 43
SE-221 00 Lund
Sweden

Abstract

We present simulations done on the onset of common envelope evolution with giant donors by taking into account the mass loss through the outer Lagrange point and the forming of the common envelope. In addition we apply proper stellar models and evolve our simulations using an Runge-Kutta integrator with adaptive step-size. We show that each of these processes are significant in the onset of common envelope evolution. The mass loss through the outer Lagrange point has significant effect, if the atmospheric scale height is high (as is the case for red giants $H_p = 0.01R_*$). In addition to this we find that subgiants with a scale height of about $H_p = 0.1R_*$ can have a stable mass transfer period during its evolution and can as a result exhaust its envelope before starting Roche lobe overflow. The nature of the mass transfer is found to be heavily dependent on the atmospheric scale height of the star. As different scale heights lead to very different evolutionary paths for the mass transfer. We also make comparisons with the conservative case and show that simple stability analysis of unstable mass transfer do not concur with the non-conservative case. We discuss the standard application of the alpha formalism and show that there are severe flaws in using it at the start of Roche lobe overflow, as opposed to at the start of common envelope evolution for giant donor stars.

Popular Abstract

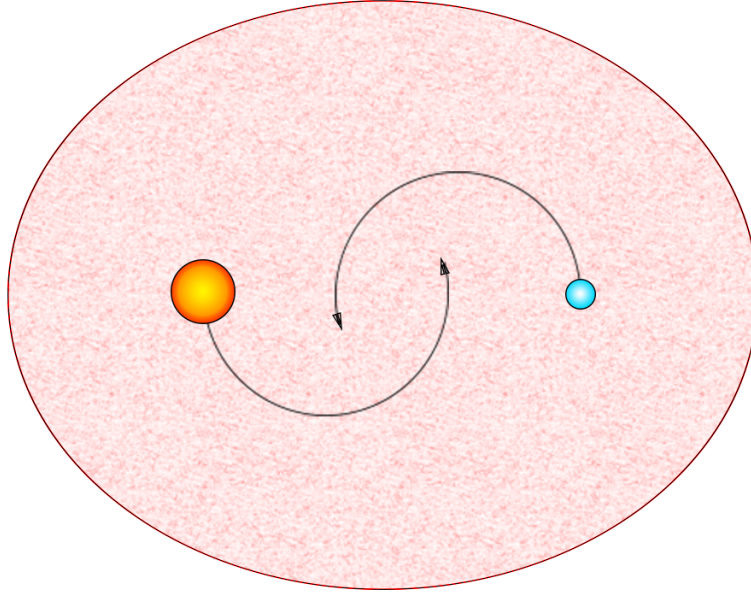


Figure 1: Illustration of a common envelope system. Here the common envelope have fully engulfed both of the stars, which are rapidly spiraling together.

A binary star system contains two stars which orbits each other around their common center of gravity. In the past it was thought that binaries were quite rare; but as our instruments of observation got better and better we found that the universe is teeming with them. The stars in a binary usually evolve independently and follow simple and similar physics as that of our own solar system. However a big difference arises if the separation between the two stars are sufficiently small that the individual evolution of each star leads to the initiation of mass transfer. As a consequence to mass transfer, a binary system can evolve through several evolutionary paths and result in some of the most exotic astronomical objects seen in the night sky.

The mass transfer that unfolds can either be stable or unstable. A stable mass transfer will slowly transfer mass from one star to the other. But an unstable mass transfer will quickly go out of control and pour its material on to the other star. However a star can only accept a finite amount of material at once and this results in the buildup of an envelope that can eventually engulf both stars. The system has now become a common envelope system. Due to frictional processes the stars spiral together and the final product will either be a tighter binary or a merger between the two stars.

An interesting product of common envelope evolution is a cataclysmic variable star, which are the predecessors to Type Ia supernova explosions. These are very important in astronomy as they are standard candles that have a specific brightness associated with them. They are used to calculate the distance to very distant objects. So as we can see it becomes quite essential to understand and investigate the physics of common envelope evolution.

This bachelor thesis will focus on the onset of common envelope evolution. We will investigate under what conditions it occurs and how likely they are to happen. Simulations are done on the onset of common envelope evolution and we discover what processes play a major role in it. Finally we will apply a method for evolving the system through its common envelope evolution and discover the final state of the binary.

Contents

1	Introduction	2
2	Method	4
2.1	Parameters	4
2.2	Integration of parameters	6
2.2.1	Numerical Integrator	7
2.3	Assumptions	7
3	Testing	9
3.1	Stable or Unstable	9
3.2	Conservative mass transfer	12
4	Processes	16
4.1	Mass loss from the outer Lagrange point	16
4.2	Eddington limit	18
4.2.1	Forming of the envelope	18
4.3	Common envelope evolution	20
5	Results	22
6	Summary and conclusions	31
A	Stellar Model	34

Chapter 1

Introduction

Common envelope evolution (CEE) is a phase in the life of binary stars, in which the two stars are engulfed in a mutual envelope. Due to frictional processes the orbit is drastically decayed until either the envelope is ejected, leaving a tight orbit, or the two stars merge. Here lies the problem in our current understanding of CEE, as our theoretical models still can't accurately predict if a binary system that undergoes common envelope evolution will result in a tight orbit or a merger. The importance of understanding this process is clear when we look at the wide array of observed systems that are believed to result from it. For example tight orbiting compact objects are important as they are the most prominent candidates to be detected by our gravitational wave detectors (like LIGO). Another resulting system is the cataclysmic variable that is made up of a white dwarf and a mass transferring companion. These are thought to be the most common progenitor of type Ia supernovas. The type Ia supernova is often used in astronomy as a standard candle to accurately measure distance to distant galaxies. The reason why we think most of these binaries results from common envelope evolution is due to the fact that these stars were once several order of magnitudes larger and would be unable to fit in the current system; which indicates that they have evolved from a large orbit to a very small one. For this to be possible within the age of the universe a quite drastic process like common envelope evolution is required. So as we can see, there is a clear interest in developing accurate models to account for the formation rate of such binaries.

In the last few decades there has been quite a lot of research done on common envelope evolution. But as the problem involves several complex physical processes there is no comprehensive solution to the problem. The most prominent early work assumed that the orbital energy was the main culprit in ejecting the envelope (van den Heuvel (1976)). This led to the α formalism by Webbink (1984) that derived the final separation of the orbit by comparing the loss in orbital energy to the binding energy of the envelope. However it is evident that the α formalism neglects certain physical processes and has been shown to be unable to accurately predict the resulting binaries. Nelemans and Tout (2005) showed that the α formalism could not be used to explain the evolution of a handful of double white dwarf binaries, as most of them would require additional energy to be generated during the common envelope phase. It is still uncertain what these extra energy sources are; but several possible candidates have been proposed. For example internal, recombination and accretion energy can all work as additional energy sources to push the envelope away. But it is still uncertain if they contribute enough on a dynamical timescale. However if the timescale for common envelope evolution is non dynamical we will not have energy conservation and the alpha formalism breaks down completely. To accurately explain these double white dwarf binaries the so called γ formalism was constructed, which is based on the conservation of angular momentum instead. The γ formalism seem promising but it has only been shown to correctly model a handful of common envelope systems, so its usefulness is still unclear.

There have been many attempts to make a 3D model of common envelope systems. Some of the more modern 3D models were made by Passy et al. (2012) which used the grid-based code Enzo in combination with the smoothed particle hydrodynamic code SPNSPH. Another model was made by Ricker and Taam (2008) which used the grid-based adaptive mesh refinement code FLASH. However modeling common envelope evolution with 3D models often comes with a bunch of problems. For example Eulerian grid-based methods suffer from conservation of angular and linear momentum due to the advection term in the hydrodynamic equation. Smoothed particle hydrodynamics often lack the necessary resolution to fully capture the physics of CEE. And the use of artificial viscosity diffuse shock fronts which makes it difficult to model sharp shock fronts that can play an important role. However smoothed particle hydrodynamics should be able to produce a good model for the onset of common envelope evolution (unless we have very slow mass transfer).

The α and γ formalism's are not usually applied when common envelope evolution starts, rather they are applied when Roche lobe overflow occurs. Here they assume that the mass transfer is conservative and that the common envelope will be as massive as the donor star's envelope when it fills its Roche lobe. However this reasoning can be problematic for stars with very thin atmospheres, as it is possible to have mass loss through the outer Lagrange point during dynamical mass transfer. Another problem is that star's with thin atmospheres can have significant mass loss before Roche lobe overflow which means that the envelope will be more massive than predicted. In this paper we will investigate the onset of common envelope evolution and take a closer look at the significance of mass loss through the outer Lagrange point and also see how much mass is lost before we reach Roche lobe overflow. We will apply the α formalism when common envelope evolution begins, instead of doing it beforehand. During this investigation we will look at different kinds of star's with different atmospheric scale heights and see if there are any significant change in the evolution.

In the second chapter we review how the simulations were done, what parameters and equations were used and what assumptions were made. The third chapter investigate the stability and the evolution of conservative mass transfer. In chapter 4 we will introduce non-conservative processes during mass transfer, this includes mass loss from the outer Lagrange point and the forming of the common envelope. At the end of the chapter we also go through the alpha-formalism. In chapter 5 we present our findings and results. Finally in chapter 6 we summarize the paper and discuss our results. The stellar model used for our non-conservative simulations have been included in Appendix A at the end of the paper.

Chapter 2

Method

We investigate the onset of common envelope evolution by solving the equations that govern both conservative (no mass loss from system) and non-conservative mass transfer in a binary. This include evolving the mass transfer rates of both stars and the response that mass transfer has on the orbit and the stars. The equations are solved analytically, numerically and are evolved using a fourth order Runge-Kutta integrator.

To get a better picture of the binary we can look at Fig. 2.1 which shows the state of a binary($q_0 = 2$) just before mass transfer begins. The parameters used in the simulations are listed in section 2.1. And the equations for the conservative and non-conservative mass transfer is listed in section 2.2. We also list the assumptions and approximations made for our simulations in section 2.3. More details on the parameters and equations will be reviewed in the following chapters when we discuss the different processes.

2.1 Parameters

Below we list the parameters used in our simulations:

M_1 – The donor star mass

M_2 – The accretor mass

a – The orbital separation

R_* – The radius of the donor star

$R_L = ar_L(q)$ – The radius of the Roche lobe

$R_{L3} = ar_{L3}(q)$ – The radius of the outer Lagrange surface

M_{Env} – The common envelope mass

M_c – The mass of the donor star's core

$H_p = \kappa R_*$ – The atmospheric scale height of the donor star

$M = M_1 + M_2$ – The mass of the two stars

$q = \frac{M_1}{M_2}$ – The mass ratio

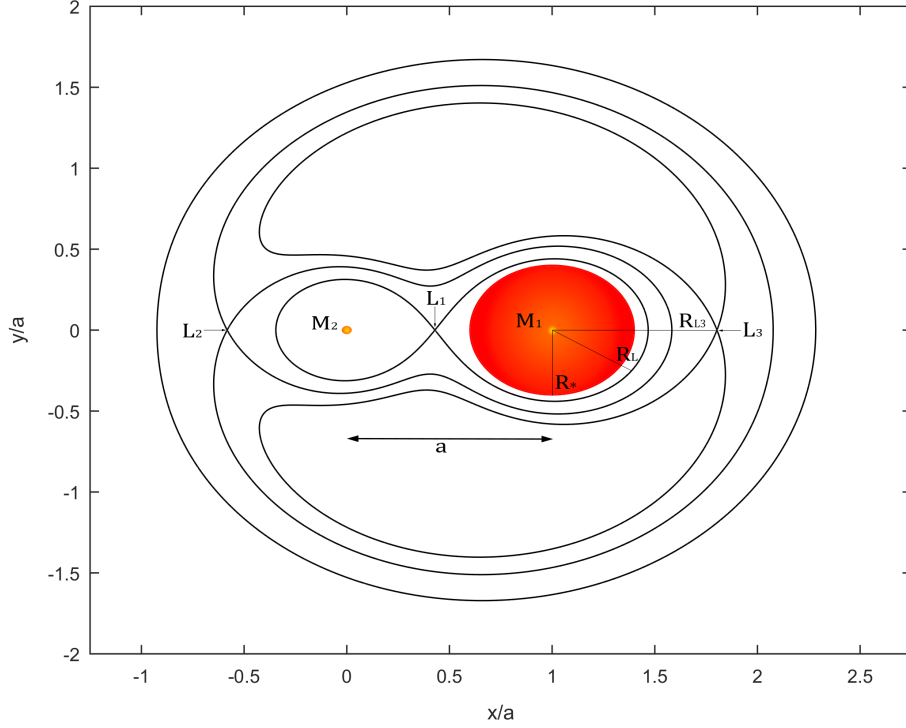


Figure 2.1: Depicts a binary with a mass ratio of $q = 2$ in its x - y plane just before mass transfer begins. The lengths have been scaled by the orbital separation a . The solid lines represent the equipotential surfaces which go through the Lagrange points (L_1, L_2 and L_3) in which the potential gradient is: $\Delta\Phi = 0$.

The radius of the Roche lobe is approximated from a sphere with the same volume as the actual Roche lobe. We use the Eggleton fitting formula (Eggleton (1983)):

$$r_L(q) = \frac{R_L}{a} = \frac{0.49q^{2/3}}{0.6q^{2/3} + \ln(1 + q^{1/3})} \quad (2.1)$$

A similar fitting function is used to approximate the radius of the outer Lagrange point (Church (2015)):

$$r_{L3}(q) = \frac{R_{L3}}{a} = \frac{0.53188q^{2/3}}{0.38266q^{2/3} + \ln(1 + q^{1/3})} \quad (2.2)$$

For the conservative case the radius of the star is approximated by using the following fitting formula (Church (2015)):

$$R_{*,j=0} = R_{\odot} \left(\frac{M}{M_{\odot}} \right)^{\gamma} \quad \gamma = \text{adiabatic index of the star} \quad (2.3)$$

For the non-conservative case a stellar model is applied (see appendix A for more detail):

$$R_* = 1.1M^{-0.3}(L^{0.4} + 0.383L^{0.76}) \quad (2.4)$$

To get the final separation of the system, the alpha formalism is applied and the following equation is used (see more details in chapter 4.4):

$$a_f = \frac{a_i}{\frac{2Mm_{env}a_i}{m_2m_c\alpha\lambda R_{env}} + 1} \quad (2.5)$$

2.2 Integration of parameters

The following differential equations are all evolved using a fourth order Runge-Kutta integrator with adaptive step-size.

Conservative mass transfer:

The rate of mass transfer from the donor star can be approximated as: (Ritter (1988))

$$\dot{M}_{1,j=0} = -\dot{M}_0 \times \exp \frac{R_L - R_*}{\kappa R_*} \quad (2.6)$$

Where \dot{M}_0 is the approximated mass transfer rate at the start of Roche lobe overflow.

$$\dot{M}_0 \approx 10^2 M_\odot yr \quad (2.7)$$

$$\dot{M}_2 = -\dot{M}_1 \quad (2.8)$$

By combining the orbital angular momentum of the binary with Keplers third law and applying the conservative case ($\dot{J} = 0 \dot{M} = 0$) we get an expression for the change in the orbit (see chapter 3.1 for more details.):

$$\dot{a} = -2a \left(\frac{\dot{M}_1}{M_1} + \frac{\dot{M}_2}{M_2} \right) \quad (2.9)$$

Non-conservative mass transfer:

Same as the conservative case but with the inclusion of mass loss through the outer Lagrange point and the build up of the envelope.

$$\dot{M}_1 = \dot{M}_{1,j=0} + \dot{m}_{L3} \quad (2.10)$$

The rate of mass loss \dot{m}_{L3} is modeled the same as $\dot{M}_{1,j=0}$ but with R_L replaced with R_{L3} .

$$\dot{m}_{L3} = C \times \exp \frac{R_{L3} - R_*}{\kappa R_*} \quad (2.11)$$

The maximum mass transfer rate for the accretor is set by the Eddington limit(see section 4.2).

$$\dot{M}_2 = -\max[\dot{M}_{edd}, \dot{M}_{1,j=0}] \quad (2.12)$$

If the mass transfer rate reaches the Eddington mass limit, the rest of it is transferred to the envelope. However the envelope can only begin to build if the gravitational binding energy of the incoming mass is larger than the outward pressure generated by the accretor:

$$\epsilon = \dot{E}_{env,bind} - \alpha \dot{E}_{edd} \quad (2.13)$$

α is the amount of kinetic energy that is absorbed by the envelope. For all our simulations $\alpha = 1$.

$$\dot{M}_{env} = \begin{cases} -\dot{M}_{1,j=0} - \dot{M}_2 & \epsilon > 0 \\ 0 & \epsilon \leq 0 \end{cases} \quad (2.14)$$

The change in the orbit is derived in section 4.2.1 and includes the effect of the non-conservative processes. The envelope is seen as semi-detached, and as such mass transfer to it will carry away orbital angular momentum from the binary.

$$\dot{a} = a \left(\frac{\dot{M}_{env}}{M} - 2\dot{m}_2 \left(\frac{m_2 - m_1}{m_1 m_2} \right) \right) + \dot{a}_{L3} \quad (2.15)$$

$$\dot{a}_{L3} = 2a \frac{\frac{dJ_{L3}}{dm_{L3}} \dot{m}_{L3}}{J} \quad (2.16)$$

2.2.1 Numerical Integrator

The change in angular momentum due to mass loss through the outer Lagrange point $\frac{dJ_{L3}}{dm_{L3}}$ is numerically integrated using Matlab's inbuilt integrator (more details in section 4.1).

$$\frac{dJ_{L3}}{dm_{L3}} = Gm_1 \int_0^\infty \left(\frac{-a^2 + a \cos(\omega t)(R_o + vt)}{(4(a^2 - a \cos(\omega t)(R_o + vt)) + (R_o + vt)^2)^{3/2}} \right) dt \quad (2.17)$$

The step-size is adapted by taking the minimum of several parameter's characteristic time scales. To further ensure the accuracy of the simulation we implement a tuning factor to the time-step condition which we set to $k = 10^{-4}$.

$$t_x = k \frac{x}{\dot{x}} \quad (2.18)$$

$$\delta t = \min[t_{m_1}, t_{R_*}, t_a] \quad (2.19)$$

2.3 Assumptions

An isolated binary will eventually reach a tidal equilibrium when it has reached its minimum energy for a specific angular momentum. This will occur when the orbit has been both circularized and synchronized. In other words a binary will strive to make its orbit circular and to synchronize their angular spin velocity to their angular orbital velocity ($\omega = \Omega$). Which is the most energy efficient configuration for an isolated binary. This assumption is justified, as the timescale for tidal equilibrium is much shorter than that of the nuclear timescale (Eldridge and Tout (20XX)). Unless there has been a drastic change in angular momentum due to winds or some other phenomena, we have already reached tidal equilibrium at the start of mass transfer. As the moment of inertia is much greater for the orbit than that of the star, the spin angular momentum for synchronized stars will be much lower than the orbital angular momentum at the start of mass transfer. Therefore we can justifiably neglect the effect of the stellar spin.

When deriving the rate of mass transfer Ritter (1988) assumes that the flow can be seen as isothermal and that only the outermost layers of the star is affected by the mass loss and that deeper layers remain stationary. For $R_L > R_*$ and for relatively slow mass transfer this approximation holds up quite well even for adiabatic stars with deep convective envelopes (Kolb and Ritter (1990)). But when the mass transfer ramps up this becomes more problematic as deeper layers are affected and the adiabatic nature of the star becomes more apparent as the speed of the accreted material will reach much higher velocities. However our formula still capture the essence of the mass transfer and will provide a good approximation together with a good choice of constant. To retain a dynamical mass transfer during Roche lobe overflow we choose this constant to be $\dot{M}_0 = 10^2$ (this is discussed in more detail in section 3.2). We also apply this same assumption to the outer Lagrange point.

In deriving the Eddington limit in section 4.2.1 we assume that the star is radiating isotropically and that the star consist of pure ionized hydrogen. For metal poor stars which we assume in our stellar model(see appendix A) this is a good approximation.

The Roche lobe radius is approximated to be the radius of a sphere with the same volume as the Roche lobe. With the Eggleton fitting function r_L (equation 2.1) this is accurate to better than one percent over the whole range of mass ratio's.

There are several processes which we neglect during our simulations. We neglect the mass loss from the system due to stellar winds, as this was deemed insignificant during the range of orbital separation that we are interested in. For the same reason orbital decay due to gravitational wave emission is also deemed insignificant. There is also the effect of magnetic braking which we also neglect. Magnetic braking is a process that occurs when magnetically coupled surface material

leaves the star. Thus the material is forced to be in co-rotation with the star as it is lost. This results in an additional angular momentum loss for the binary. The details of magnetic braking still remain quite uncertain and that is why we have ignored it in this paper. However an upcoming article by Pavlovskii and Ivanova (2016) indicate that its effect should play an important role in the mass transfer of giant donors.

Chapter 3

Testing

This testing chapter was made to investigate the stability criterion and evolution of conservative mass transfer in a binary, and act as a comparison measure for the non-conservative simulations done in the results chapter.

3.1 Stable or Unstable

The Roche lobe is an equipotential surface around each of the stars which are joined together at the first Lagrange point L_1 (Fig. 2.1). If material goes beyond this surface it will be more attracted to its companion star and mass will be transferred from one star to the other. The radius of the Roche lobe is approximated from a sphere with the same volume as the actual Roche lobe:

$$R_L = ar_L(q)$$

Were r_L is a fitting function of the mass ratio $q = M_1/M_2$. Here we have taken M_1 to be the donor star and M_2 as the accretor. We will compare two different fitting functions (r_L) in this section to see how much the result differ. The first is the Paczynski approximation formula (Paczynski (1971)) which is often used when doing analytic work:

$$r_{Lpac}(q) = 0.46224 \left(\frac{M_1}{M} \right)^{1/3} \quad (3.1)$$

The second is the Eggleton approximation formula (Eggleton (1983)) shown in equation 2.1 (we will label it as r_{Legg} in this section) which is more often used in numerical work and the one that we will use for our simulations.

Mass transfer can either be stable or unstable. If the mass transfer is stable the radius of the Roche lobe will grow faster than that of the donor star and the rate of mass transfer will eventually be governed by the slow degradation of the orbit due to external influences. For example gravitational wave emission from the binary. However if the radius of the donor star grows faster than that of the Roche lobe in response to mass loss; we will have an unstable mass transfer. This is due to the fact that as we lose mass the more material will become unbound from the donor star which leads to an exponential increase in the mass rate.

The radius of the donor star is approximated using equation 2.3. To investigate at what mass ratio the mass transfer becomes unstable we compare how the star and the Roche lobe reacts to mass loss.

$$\xi_* = \frac{\partial \ln R_*}{\partial \ln M_1} = \gamma \quad (3.2)$$

$$\xi_L = \frac{\partial \ln R_L}{\partial \ln M_1} = \frac{\partial \ln a}{\partial \ln M_1} + \frac{\partial \ln r_L(q)}{\partial \ln M_1} \quad (3.3)$$

We look at the case where the total mass and the angular momentum is conserved, so any material that is lost by star 1 is accreted by star 2.

$$M = M_1 + M_2 \quad (3.4)$$

$$\dot{M}_1 = -\dot{M}_2 \quad (3.5)$$

To figure out how the orbital separation changes we can use the total angular momentum for the binary which can be written as (Eldridge and Tout (20XX)):

$$H = I\Omega + \mu a^2 \omega = \text{constant} \quad (3.6)$$

The first term is the spin momentum and the second the orbital angular momentum. I is the moment of inertia, $\mu = \frac{M_1 M_2}{M}$ is the reduced mass and ω is the orbital angular velocity and Ω is the spin angular velocity. As mentioned in section 2.3 an isolated binary will, due to synchronization, move towards an equilibrium in which the orbital angular velocity is equal to the spin angular velocity. The total angular momentum can then be approximated as:

$$H = \omega_{eq}(I + \mu a^2) \quad (3.7)$$

The orbital angular momentum is equal to:

$$J = \mu a^2 \omega \quad (3.8)$$

Differentiating this with respect to time and combining it with Keplers law we get an expression that looks like:

$$\frac{\dot{a}}{a} = \frac{\dot{M}}{M} - 2\left(\frac{\dot{M}_1}{M_1} + \frac{\dot{M}_2}{M_2} - \frac{\dot{J}}{J}\right) \quad (3.9)$$

In the conservative case ($\dot{J} = 0$, $\dot{M} = 0$) we end up with equation 2.9 which then after integrating gives us:

$$a = \frac{K}{(M_1 M_2)^2} \quad (3.10)$$

Where K is just a constant.

After some algebra we can calculate $\frac{\partial \ln r_L(q)}{\partial \ln M_1}$ for both approximations:

$$\frac{\partial \ln a}{\partial \ln M_1} = 2(q - 1) \quad (3.11)$$

$$\frac{\partial \ln r_{Lpac}(q)}{\partial \ln M_1} = 1/3 \quad (3.12)$$

$$\frac{\partial \ln r_{Legg}(q)}{\partial \ln M_1} = (1 + q) \left(2/3 - \frac{0.4q^{2/3} + \frac{q^{1/3}}{3(1+q^{1/3})}}{0.6q^{2/3} + \ln(1 + q^{1/3})} \right) \quad (3.13)$$

If ξ_L is larger than ξ_* the Roche lobe shrinks faster than the star does, which leads to an unstable mass transfer.

$$\xi_L > \xi_* \quad (3.14)$$

Using the Paczynski approximation:

$$1/3 + 2(q - 1) > \gamma \rightarrow q > \frac{3\gamma + 5}{6} \quad (3.15)$$

For $\gamma = -1/3$ this gives:

$$q > \frac{4}{6} \quad (3.16)$$

Its harder to get a mass ratio expression for the Eggleton approximation. But one can find the threshold mass ratio numerically. For $\gamma = -1/3$ this gives:

$$q > 0.6340 \quad (3.17)$$

Which is smaller than $\frac{4}{6}$

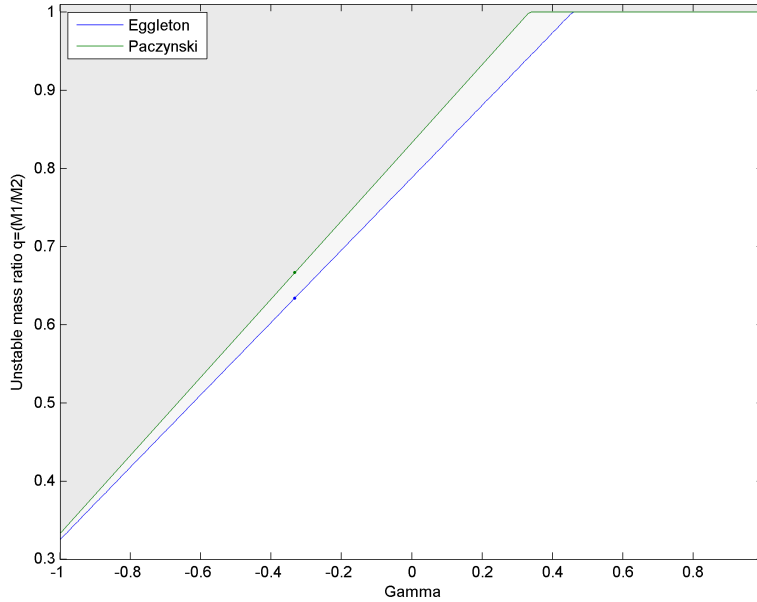


Figure 3.1: Showing the threshold mass ratio for unstable mass transfer with different γ for the star. Shaded areas are the unstable mass ratio regions. Dots show the threshold mass ratio for $\gamma = -1/3$. Comparing two approximation formulas (Eggleton and Paczynski)

From Fig. 3.1 we can see that the results indicate that the mass transfer from giants more often than not is unstable. The star that first transition over to the giant branch and reaches its Roche lobe is the more massive one. Therefore q will in most cases be larger than one. The only two cases in which stable mass transfer could occur is if the more massive star has lost a significant part of its mass before its giant phase, or the mass transfer began before the more massive star became a red giant.

3.2 Conservative mass transfer

To see how the system evolves we first take a look at the conservative case ($\dot{M}_1 = -\dot{M}_2$, $\dot{J} = 0$). The rate of mass transfer from the donor star can be approximated as: (Ritter (1988))

$$\dot{M}_1 = \dot{M}_0 \times \exp -\frac{R_L - R_*}{\kappa R_*}$$

κR_* is the scale height. It is the height over the surface in which the atmospheric pressure have dropped by a factor e . For a red giant the scale height is about $\kappa \sim 0.1R_\odot$ and for a subgiant its about $\kappa \sim 0.01R_\odot$. The constant \dot{M}_0 is the rate of mass transfer at the Roche lobe. Using the method that Ritter used in his paper to get the rate of mass transfer heavily under estimates it. The reason being that compared to Ritter we have an adiabatic flow and a much larger scale height. We do however know that the timescale for mass transfer during Roche lobe overflow should proceed on a dynamical timescale as its governed by the sudden change in potential. The dynamical timescale for a $M_* = 1M_\odot$ and $R_* = 10R_\odot$ is about $10^{-3}yr$ which corresponds to a mass transfer rate of about:

$$\dot{M}_0 \approx 10^2 M_\odot yr$$

Several simulation were done to get a general sense for how conservative unstable mass transfer behaves in a binary. These simulations will also work as a comparison tool for the non-conservative case which we present in chapter 5. The simulations make use of the conservative-case equations given in the method section (equation). The simulations, start at a separation were the initial radius of the star is the same as that of the initial radius of the Roche lobe ($R_* = R_L$). The system is evolved using an adaptive stepsize and as we have an initial mass rate of $\dot{M}_0 = 10^2 M_\odot yr$ we set the timespan to 0.01 years.

As we mentioned before the dynamical timescale is about $10^{-3}yr$ and from Fig. 3.2 we can see that the unstable mass transfer ceases around that time. To see how the mass transfer rate evolves we can take a look at Fig. 3.6 which show how the exponent in the mass transfer function evolves. We see that all the mass ratio's above 0.5 have an exponential mass transfer, while the $q = 0.5$ case maintain a stable mass transfer. This agrees with the result we got in the previous chapter were we established that only a mass ratio above 0.63 would produce unstable mass transfer during Roche lobe overflow. The spread which we see in the mass ratio's in Fig. 3.2 may then come as a surprise as we just concluded that mass transfer was stable below 0.63. But as we can see the final values are spread out and way below the value of 0.63. The reason for this can be understood if we once again take a look at Fig. 3.6. The minimums in the figure correspond to the mass rate at the threshold mass ratio of 0.63. As we can see the mass lost from ascending the trough gets larger for the systems with higher initial mass ratio. So the higher the initial mass ratio, the lower the final mass ratio becomes.

The evolution of the orbital separation can be seen in Fig. 3.3. From this figure we can see that the separations of the systems with mass ratio above $q = 1$ experience a temporary shrinkage in the orbit. This is due to the fact that in these binaries the donor star is initially more massive than its companion. Which from equation 3.14 leads to a shrinkage in the orbit until the mass ratio in the system is equal to $q = 1$, in which the orbit starts to widen instead.

From Fig. 3.4 we can see that different gamma's results in different turn off points and final mass ratio's. Which is reasonable as the mass ratio for stability increases with gamma (see Fig. 3.1). From Fig. 3.5 we can see that lower kappa speeds up the process of mass transfer. Another consequence that can be seen from Fig. 3.5 is that we have a smaller mass transfer rate before Roche lobe overflow. As a consequence the stars with a larger kappa will end up at a smaller mass ratio.

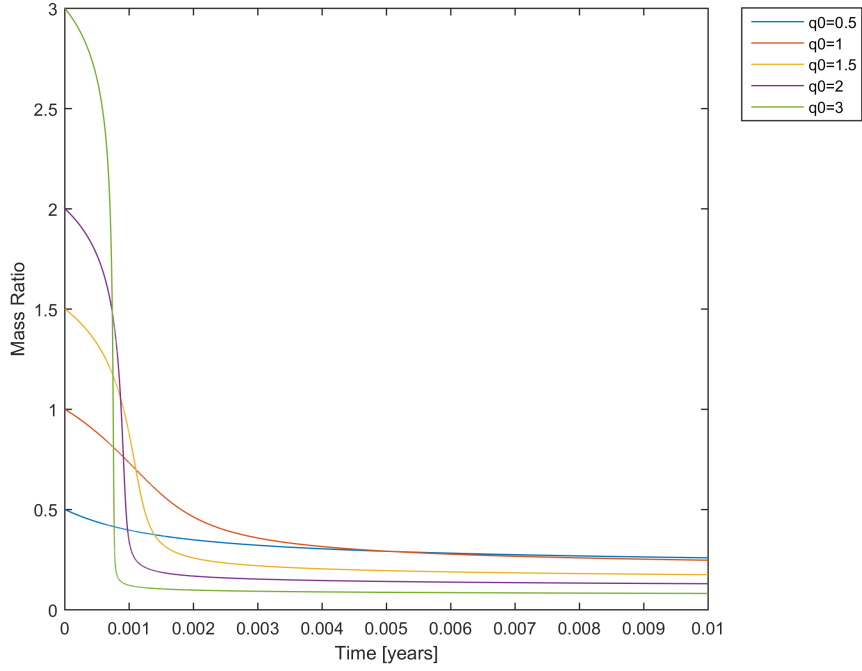


Figure 3.2: The evolution of the mass ratio in a conservative mass transfer using different initial mass ratios. With $\gamma=-1/3$ and $\kappa=0.1$. After unstable mass transfer, the final mass ratio's was: $q_{end} = [0.2592, 0.2474, 0.1753, 0.1302, 0.0817]$.

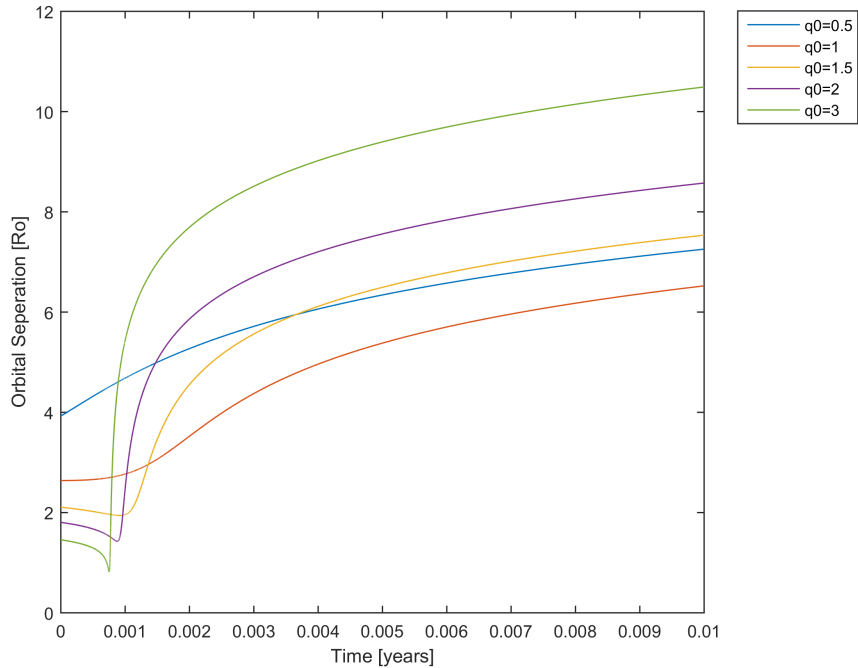


Figure 3.3: The evolution of the orbital separation in a conservative mass transfer using different initial mass ratios. With $\gamma=-1/3$ and $\kappa=0.1$.

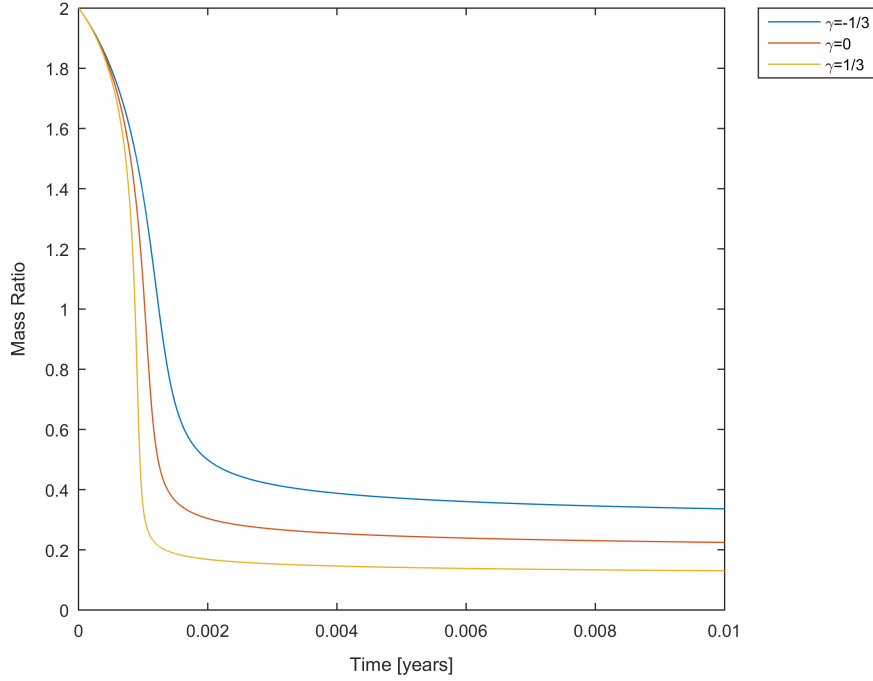


Figure 3.4: The evolution of the mass ratio in a conservative mass transfer using different γ . With $q = 2$ and $\kappa=0.1$. Final mass ratio for each respecting simulation was: $q_{end} = [0.3359, 0.2245, 0.1302]$.

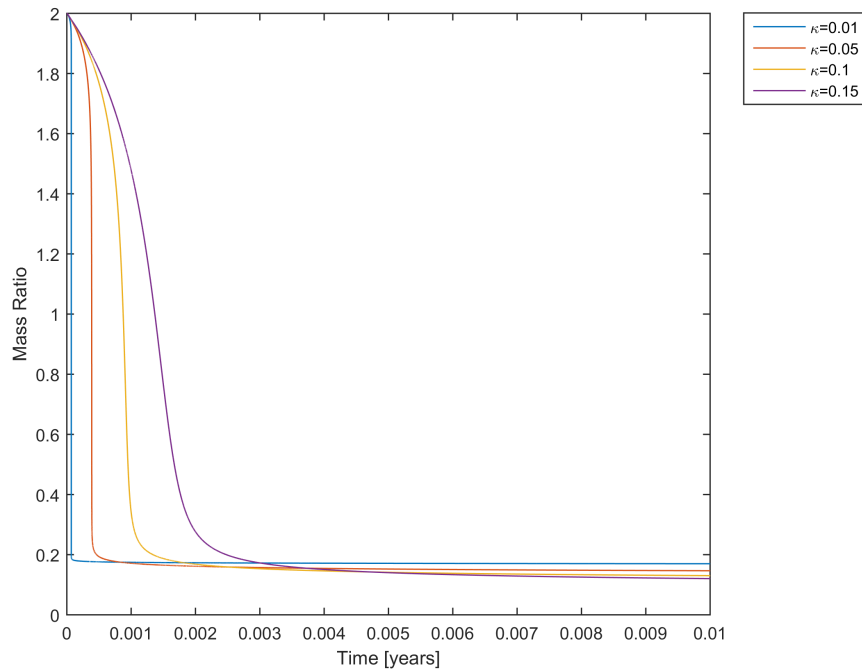


Figure 3.5: The evolution of the mass ratio in a conservative mass transfer using different κ . With $q = 2$ and $\gamma=-1/3$. Final mass ratio for each respecting simulation was: $q_{end} = [0.1698, 0.1465, 0.1302, 0.1203]$.

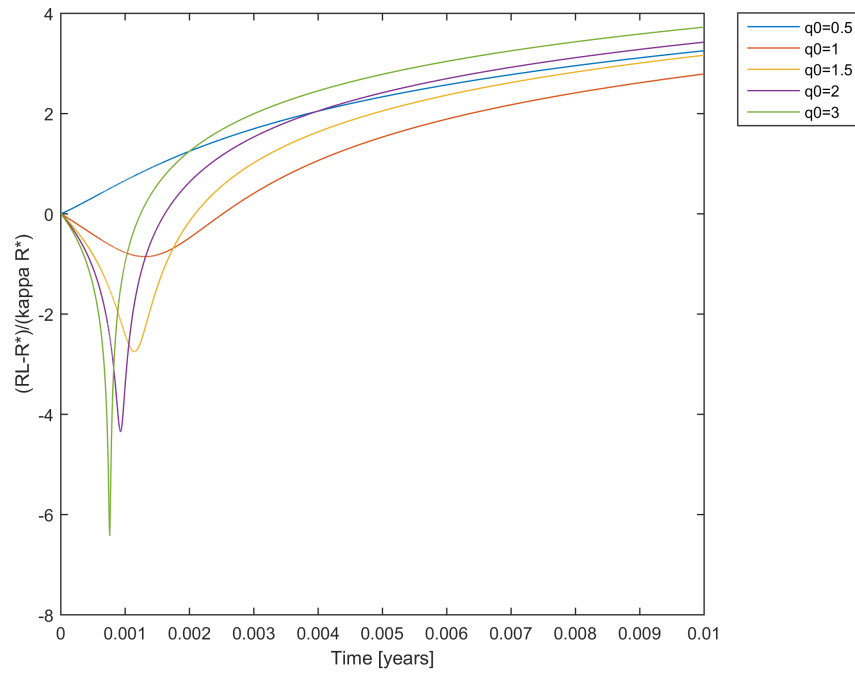


Figure 3.6: Evolution of the exponent in the mass rate function. We can see that all initial mass ratios above 0.5 experience an exponential mass loss. The minimum in the mass rate occurs at $q = 0.63$. Done with $\gamma = -1/3$ and $\kappa = 0.1$

Chapter 4

Processes

In this section we investigate the non-conservative processes that can affect the evolution of the binary during mass transfer.

4.1 Mass loss from the outer Lagrange point

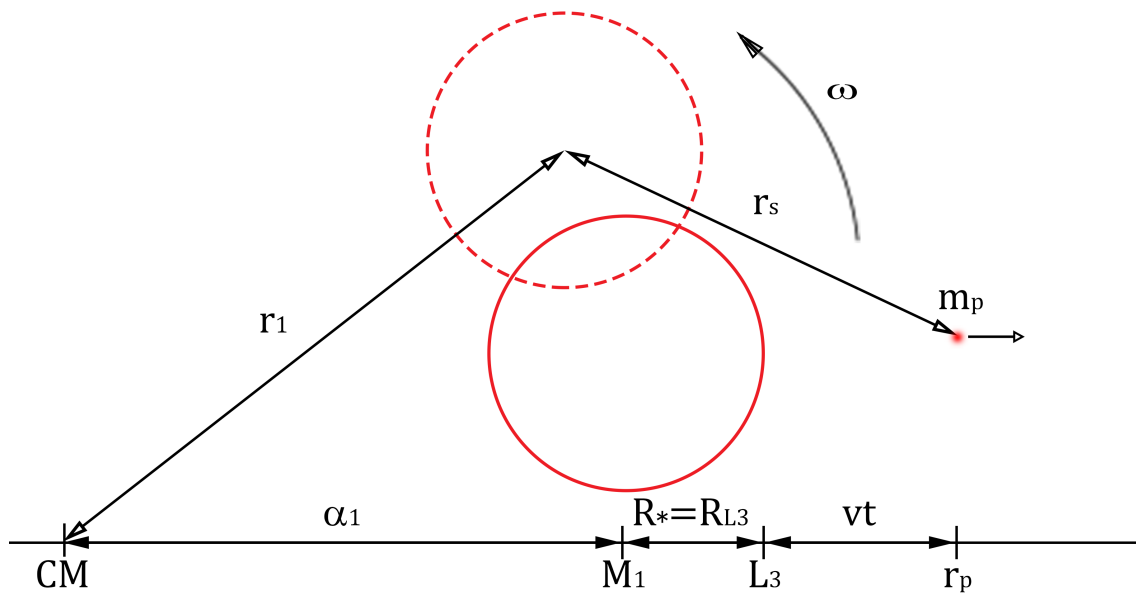


Figure 4.1: We trace the effect of a single proton leaving through the outer Lagrange point L_2 . The solid red circle represent the star at the initial time and the dashed red circle represent the star at time t . The proton will exert a torque on the star, taking angular momentum from the orbit.

If material goes beyond the outer Lagrange surface, mass will begin to leave the system and mass won't be conserved anymore. The mass that leaves the system will also take some of the angular momentum of the donor star with it. We can evaluate the significance of the angular momentum loss by seeing how much is lost by a single particle leaving the system. We imagine that a proton leaves the star with velocity v perpendicularly through the second Lagrange point as seen in Fig. 4.1. The radius of the outer Lagrange surface is given by equation 2.2. Basically

the same as the Eggleton formula but with other constants.

The torque acting on the star by the proton will be:

$$\tau = Gm_p m_1 \left(\frac{r_1 \cdot r_s}{|r_1 + r_s|^3} \right) \hat{a} \quad (4.1)$$

$$\hat{a} = [\sin(\omega t), -\cos(\omega t)]$$

$$r_1 = [a_1 \cos(\omega t), a_1 \sin(\omega t)]$$

$$r_s = r_p - r_1$$

$$r_p = [R_o + vt, 0]$$

$$R_o = a_1 + R_*$$

After some algebra on equation 4.1 we get:

$$\tau = Gm_p m_1 \left(\frac{-a^2 + a \cos(\omega t)(R_o + vt)}{(4(a^2 - a \cos(\omega t)(R_o + vt)) + (R_o + vt)^2)^{3/2}} \right) \hat{a} \quad (4.2)$$

The change in orbital angular momentum will be equal to the magnitude of the torque:

$$\Delta J = |\tau|$$

From equation 4.2 we can see that it converges as $t \rightarrow \infty$. To see what the total loss of angular momentum from a single proton is we solve this using a numerical integrator and see what value we get when it converges. We set m_1 to 2 and m_2 to 1 and use the same equations to get a and R_* as we did in the previous chapter. As we are looking at the change of angular momentum caused by an extremely small mass we can approximate this as a derivative.

$$\frac{\Delta J}{\Delta m} \approx \frac{dJ}{dm} = -2.17 \times 10^5$$

To get a better idea how significant this is we can compare with the total orbital angular momentum over the total mass:

$$\frac{J_{tot}/M}{dJ/dm} \approx 0.05$$

So approximately 5% of the total mass has to leave through the outer Lagrange point to completely diminish the orbital angular momentum. However only a fraction of this is required to cause the system to become unstable, due to the fact that the mass transfer rate through the outer Lagrange surface will increase as the orbit decays.

The derivative $\frac{dJ}{dm}$ is integrated numerically at each timestep in our simulations (see equation 2.17). And the rate of change in the separation due to the outer Lagrange point is derived from equation 3.9 and shown in equation 2.16. The rate of mass transfer through the outer Lagrange point follows the same formula as that of the Roche lobe and is shown in equation 2.11.

4.2 Eddington limit

This section follows the derivation given in Introduction to High-Energy physics by Rosswog and Brüggen (2007).

When a star accretes material, kinetic energy of the in-falling material is transformed into radiation. The rate of radiation released will then be correlated to the rate of accretion. The maximum accretion rate of a star is set by the Eddington limit. This limit corresponds to when the radiation pressure from the accreting mass is equal to the gravitational pressure. The gravitational force is:

$$F_g = \frac{GM(m_p + m_e)}{r^2} = \frac{GM(m_p)}{r^2} \quad (4.3)$$

Only the mass of the proton is important as it is so much larger than that of the electron. The force due to radiation is:

$$F_{rad} = \frac{L\sigma_T}{4\pi r^2 c} \quad (4.4)$$

σ_T is the Thomson cross section and is defined as:

$$\sigma_T = \frac{2}{3} \left(\frac{e^2}{mc^2} \right)^2 \quad (4.5)$$

Which is taken to be that of the electrons as the Thomson cross section is so much larger than that of the protons. The electrostatic attraction between protons and electrons hold them together and they experience the resulting force of both. The Eddington limit is gained by setting these forces equal and solving for the luminosity

$$F_g = F_{rad} \rightarrow L_{Edd} = \frac{4\pi GMm_p c}{\sigma_T} \quad (4.6)$$

If the luminosity becomes greater than this, it will result in an outward flow of material.

The mass rate limit depends on how efficient the accreting star is at converting gravitational energy to radiation. This rate limit can be approximated as:

$$\dot{M}_{Edd} = \frac{L_{Edd}}{\eta c^2} \quad (4.7)$$

The efficiency of conversion is $\eta = \frac{R_s}{2R}$ and R_s is the Schwarzschild radius of a black hole with the same mass as the star. We can see that it is directly proportional to the stars radius and for a MS star η is about 10^{-6} . Inserting L_{Edd} with values of the different constants gives us a rate of:

$$\dot{M}_{Edd} = 2.2 \left(\frac{M_{acc}}{10^3 M_\odot} \right) M_\odot yr^{-1} \quad (4.8)$$

M_{acc} is the mass of the accretor. This is quite a low mass transfer rate and will always be fulfilled before the start of Roche lobe overflow.

4.2.1 Forming of the envelope

If the mass transfer rate from the donor star exceeds the Eddington limit, the accretor cannot accept all the incoming mass at once and an envelope will start to form around it.

$$\dot{M}_{env} = -\dot{M}_{Edd} - \dot{M}_{1,j=0}$$

$\dot{M}_{1,j=0}$ Only include mass loss through the inner Lagrange point.

An envelope can however not begin to build if the outward pressure generated by the accretor is larger than the gravitational binding energy of \dot{M}_{env} .

$$\dot{E}_{env,bind} = \frac{G\dot{M}_{env}M}{a} \quad (4.9)$$

$$\dot{E}_{edd} = \dot{M}_{Edd}\eta c^2 \approx 3 \times 10^{13} c^2 \left(\frac{M_{acc}}{10^9 M_\odot} \right) L_\odot \quad (4.10)$$

We introduce a criterion parameter ϵ . If $\epsilon > 0$ the envelope will accumulate mass otherwise the mass is lost from the system.

$$\epsilon = \dot{E}_{env,bind} - \zeta \dot{E}_{edd} \quad (4.11)$$

ζ is the amount of kinetic energy that is absorbed by the envelope. For all our simulations $\zeta = 1$.

The envelope can be seen to be semi-detached from the binary, which means that mass transferred to the envelope will carry away orbital angular momentum from the binary. As we assume that the spin of the donor star is insignificant (see section 2.3) we can calculate the rate of angular momentum as:

$$\dot{J} = -\dot{M}_{env} a_1^2 \omega \quad (4.12)$$

a_1 is the distance from star 1 to the center of mass in the system.

$$a_1 = \frac{aM_2}{M} \quad (4.13)$$

To calculate the change in separation due to mass transfer to the envelope we need to go back to equation 3.12 and solve for the non-conservative case. Combining equation 3.8, 3.9, 4.13 and 4.14 we get after some algebra ($\dot{M} = -\dot{M}_{env}$):

$$\frac{\dot{a}}{a} = \frac{\dot{M}_{env}}{M} - 2\dot{m}_2 \left(\frac{m_2 - m_1}{m_1 m_2} \right) \quad (4.14)$$

From this we can see that we have an increase in orbital separation as the system transfers mass to the envelope. Which means that we increase the stability of the mass transfer when we transfer mass in this fashion. We can see that the second term reduce to the same equation we had in the conservative case and that it contains the same properties as it (that is to say it has a minimum when $m_1 = m_2$).

If we also include the effect of mass loss through the outer Lagrange point, we get the complete equation of the rate of change in the orbital separation which is given in equation 2.15.

4.3 Common envelope evolution

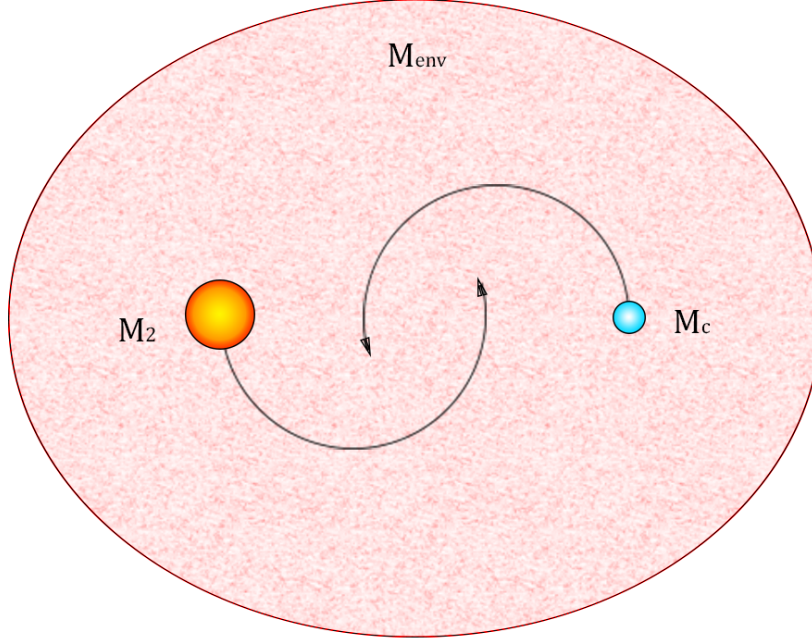


Figure 4.2: The figure depicts the state of the binary during common envelope evolution. The donor star has been stripped naked and only its core remains within the common envelope. The orbit will rapidly decay due to frictional drag until either the stars merge or the envelope is blown away.

The common envelope phase will start either when the donor star has transferred its whole envelope or when its companion star gets swallowed by it. If the second case occurs the total envelope mass becomes the sum of the current accumulated common envelope and the donor star's envelope.

When the common envelope phase starts we apply the alpha energy formalism (Webbink (1984)). As we mentioned in the introduction the alpha formalism derives the final separation of a common envelope system by comparing the loss in orbital energy to the binding energy of the common envelope. Unlike Webbink, who evolved the system from the start of Roche lobe overflow, we will instead use the alpha formalism when the common envelope phase begins. In the standard case the envelope is only bound to the donor star while in our case the envelope is bound to the whole system. So small alterations have been made to account for this.

$$\frac{GM M_{env}}{\lambda R_{env}} = \alpha \left(-\frac{GM_c M_2}{2a_i} + \frac{GM_c M_2}{2a_f} \right) \quad (4.15)$$

α is the efficiency in which the orbital energy is transferred to the envelope during CEE. In our simulations we assume that all of the orbital energy is transferred to the envelope ($\alpha = 1$). λ is a constant that accounts for the structure of the common envelope. As we do not exactly know how the density distribution of the envelope looks like we assume that its structure is similar to the envelope of a red giant which de Kool (1990) found to be around $\lambda = 0.5$. R_{env} is the radius of the envelope. We break out the final separation a_f from equation 4.16 and get:

$$a_f = \frac{a_i}{\frac{2MM_{env}a_i}{M_2M_c\alpha\lambda R_{env}} + 1}$$

The radius of the envelope is set to the orbital separation $R_{env} = a$.

To determine the resulting fate of the binary after common envelope evolution we compare the final separation to the sum of radius's of the two stars.

$$\beta = a_f - (R_c + R_2) \quad (4.16)$$

We approximate the core of the donor star to be about the radius of a white dwarf (from Hurley et al. (2000)).

$$R_c = \max[R_{NS}, 0.0115 \sqrt{\left(\frac{M_{CH}}{M_c}\right)^{2/3} - \left(\frac{M_c}{M_{CH}}\right)^{2/3}}] \quad (4.17)$$

We use equation 2.3 for R_2 with gamma set to 1/3 which is reasonable for a MS star. If $\beta < 0$ the final result is a merger otherwise it is not.

Chapter 5

Results

All the processes discussed in the previous chapter have been included in these simulations. To properly simulate the forming of the common envelope and determine the start of CEE we add a more extensive stellar model (see appendix A for more details). The simulation is started at the separation in which the mass rate is equal to 0.1 of the Eddington mass rate limit. This is before any of the processes discussed in chapter 4 have any significance. The simulation is stopped when the CEE begins, that is when either the donor star exhaust its envelope ($M_c == M_1$) or when the secondary gets swallowed by the donor ($R_* => a$). The simulation is also stopped if the rate of mass transfer becomes too small $\dot{M}_1 <= 10^{-8} M_\odot/year$ at this point the system is deemed to be stable. When the simulation is stopped the parameters at that point are entered into the alpha formalism (equation 2.5) to evolve the system through the common envelope phase. Then we check if the final separation represents a merger between the two stars (equation 4.16). Finally we also wanted to look at the difference in applying the alpha prescription at the start of Roche lobe overflow compared to the start of CEE. To do that we just take the values that we have when Roche lobe overflow begins and apply the alpha prescription.

Two scale heights were used for the simulations, $\kappa = 0.01$ and $\kappa = 0.1$ over a large range of mass ratios and secondary masses. The final separations of these systems are given in table 5.1 and 5.3. A logarithmic plot of these values can be seen in Fig. 5.5 and 5.6 for each respective scale height. The final separation values when applying the alpha formula when Roche lobe overflow starts are shown in table 5.2 and 5.4. Blank spaces in these tables represent system's in which the Roche lobe was not reached and therefore no comparison could be made.

We begin to look at the case with a small scale height $\kappa = 0.01$. To get a better picture on how the system evolves lets look at two example system's that behave quite different in this case. The $q_0 = 1$ $M_2(t = 0) = 1$ system seen in Fig 5.1 evolves similar to what one would expect. That is the mass rate is evolving exponentially just as it did in the conservative case (Fig. 3.6). Almost all of its mass is transferred during its dynamical mass transfer period and its final separation becomes $0.49R_\odot$ which corresponds to a merger. The $q_0 = 5$ $M_2(t = 0) = 1$ system seen in Fig 5.1 start to evolve exponentially, but faster than in the previous system. This is reasonable as we saw the same happen for the conservative case. However this exponential growth is suddenly stopped and a plateau in the mass transfer rate proceeds. This happens when the Roche lobe is changing at the same rate as the star which can be seen in Fig. 5.2. During this equilibrium plateau we have stable mass transfer which is at about $\dot{M}_1 \approx 5 \times 10^{-2} M_\odot yr^{-1}$. If one takes a closer look at the plateau we can see that it is not completely flat and that the mass rate during this time actually goes down for awhile until it eventually turns around and quickly becomes unstable. But as we can see from Fig. 5.1 this occurs quite late for the $q_0 = 5$ system, and by then most of the mass has already been lost. The system does not even experience Roche lobe overflow. During the time on the plateau the orbital separation is widened and because the mass transfer rate to the envelope is quite slow during this time, most of the mass is blown away by the outward pressure

of the accretor (see equation 2.13). This means that even after the donor star has exhausted its envelope there is no common envelope phase for this system; and the final separation becomes $a_f = 1050R_\odot$. which is a wider separation than the initial one. When looking at Fig 5.1 we can see a correlation between the mass ratio to the time spent on the plateau phase.

Table 5.1 shows that we have quite a linear growth as we increase the mass ratio. We can also see that we get more mergers the smaller our companion mass is. In Fig. 5.6 it is however revealed that, even if we in general have a linear growth there exist regions on the line that behave differently. These regions appear for all of the cases except $m_2 = 0.25$, however they may appear if we would increase the mass ratio range. As all cases have them we will only take a closer look at one of them ($m_2 = 1$). Most of these regions can be explained by looking at Fig. 5.7 which shows how much mass is lost from the system for mass ratios within the different regions. Because the scale height is small the mass loss through the outer Lagrange point is insignificant and plays no role. First, between ($q = 1 \rightarrow 2$) we have the cases that behave similar to the conservative case and we have practically no mass loss from the system. Second we have our first transitional region between about ($q = 2 \rightarrow 2.5$) that occur because the systems enter the plateau phase and are starting to have an increased mass loss due to the outward pressure generated by the accretor (equation 4.11). The next section ($q = 2.5 \rightarrow 3.1$) is more complicated but basically have different periods in which mass is accumulated to the envelope and others in which it is lost (see Fig 5.7). Then between ($q = 3.1 \rightarrow 5.2$) we have a linear growth, which is when there is no build up of the envelope during its plateau phase and only some when it starts to fall off (as in the $q_0 = 5$ case described before). The final region ($q = 5.2 \rightarrow 6$) represent when all the mass is lost during the plateau phase.

The difference in applying the alpha formalism at the Roche lobe compared to at the start of CEE can be seen in table 5.1 and table 5.2 for $\kappa = 0.01$. Here we can see that we get smaller final separations if we apply it at the Roche lobe which is reasonable as evolving it further only makes it either widen its orbit or lose more of its envelope. The differences is not that big for most cases but as we can see from table 5.2 there is a bigger difference when we have a high companion mass and low mass ratio. There are also quite a few cases that does not even reach the Roche lobe.

The case with a larger scale height $\kappa = 0.1$ the evolution of the system behaves very differently. In this case the mass transfer will be much higher before we reach Roche lobe overflow. This means that a common envelope can start to form earlier and that mass loss through the outer Lagrange point plays a much larger role. The significance of mass loss through the outer Lagrange point becomes quite apparent when we see the drastic orbital decay that can be seen in Fig. 5.4. This case is much more complex than the former one, which is clear when looking at table 5.3 that seem to have a much more irregular pattern than the linear one we saw in table 5.1. However if we look at Fig. 5.5 a pattern emerges and from the figure we can depict 2 different evolutionary paths. The first descent in the beginning of the figure is the transition from system's with stability to ones that go into a common envelope phase. However these system's enter their common envelope phase before they reach Roche lobe overflow. The second rapid descent depicts the transition to system's which instead go into their common envelope phase during Roche lobe overflow. The reason to the rapid descent is due to the fact that much more mass is lost to the outer Lagrange point during dynamical mass transfer. Which in turn results in more orbital decay (see Fig 5.4) and therefore a much smaller final separation. For example in the case of a secondary mass of 0.25 the mass lost from the outer Lagrange point goes from $0.0022M_o$ to $0.0544M_o$ when increasing the mass ratio of the system from 3.2 to 3.3.

The same early regions that appear in the $\kappa = 0.01$ case appear in this one. Seen in Fig 5.5 from $q = 4 \rightarrow 5$ in the $m_2 = 0.5$ case, from $q = 3 \rightarrow 3.5$ in the $m_2 = 0.75$ case, from $q = 2 \rightarrow 2.5$ in the $m_2 = 1$ case and from $q = 1.5 \rightarrow 2$ in the $m_2 = 1.25$. They occur for the same reason as in the $\kappa = 0.01$ case. During these periods the envelope mass for increasing mass ratio change very little which lead to an increase in final separation.

The difference in applying the alpha formalism at the Roche lobe compared to at the start of common envelope can be seen in table 5.3 and table 5.4 for $\kappa = 0.1$. We see that we get a larger value for the final separation when applying the alpha formalism earlier in this case. So just the opposite of the $\kappa = 0.01$ case. This is maybe a smaller difference than one would have thought. As the cases that reach the Roche lobe have significant orbital decay as a result of mass loss through the outer Lagrange point as explained before. However when applying the alpha formalism at the Roche lobe we have more mass in the system and envelope, which result in a larger binding energy (see equation 4.15).

Table 5.3 further show that the stability analysis that we did earlier in the paper does not truly hold for the non-conservative case. Further analysis reveals that the stability threshold for the $\kappa = 0.1$ case is $q_0 = 1.18$ and for $\kappa = 0.01$ it is $q_0 = 0.82$. This is way off the $q_0 = 0.63$ value that we got in section 3.1.

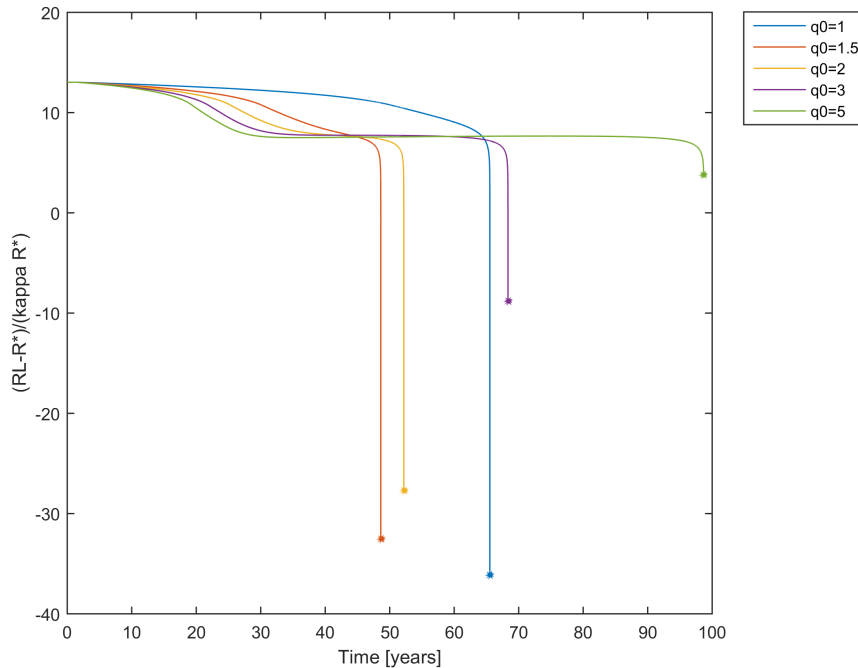


Figure 5.1: Evolution of the exponent in the mass rate function during a non-conservative mass transfer. A plateau of constant mass loss occurs at around 7, the time spent on the plateau depends on the initial mass ratio. The scale height is set to $\kappa = 0.01$.

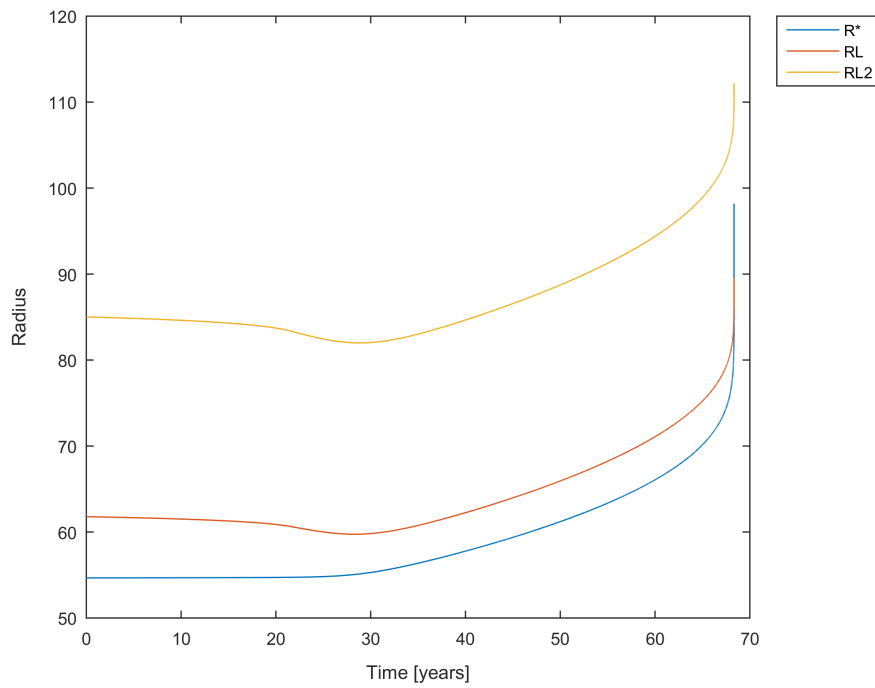


Figure 5.2: The evolution of the radius of the donor star, Roche lobe and outer Lagrange surface in a non-conservative mass transfer. The mass ratio is set to $q = 3$ and the scale height is set to $\kappa = 0.01$. From the figure we can see that the plateau in Fig. 5.1 is the result of the star and Roche lobe radius increasing at the same rate.

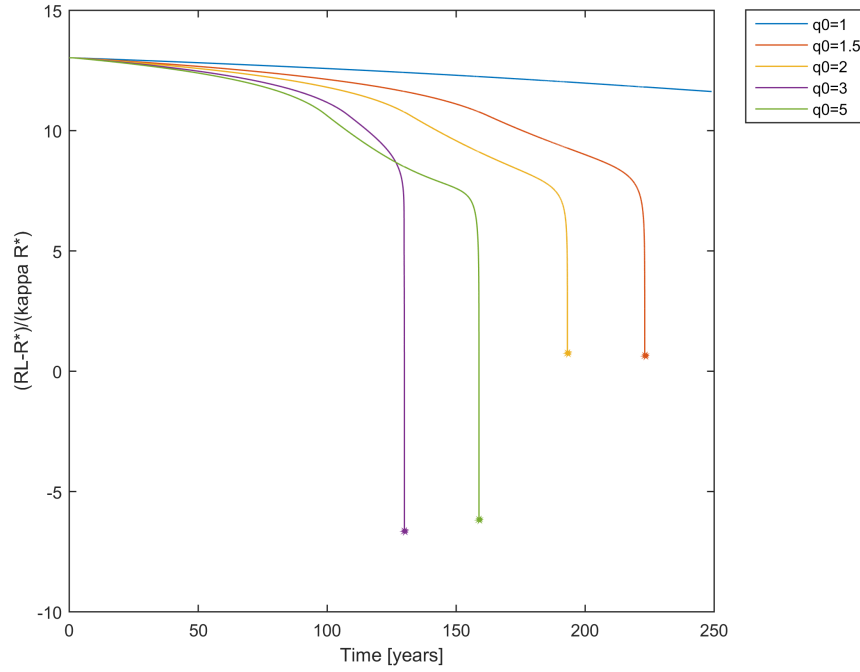


Figure 5.3: Evolution of the exponent in the mass rate function during a non-conservative mass transfer. We can see that for $q_0 = 1.5 - 2$ the mass transfer stops before Roche lobe overflow. Further evolution of $q_0 = 1$ shows that it is stable. The scale height is set to $\kappa = 0.1$.

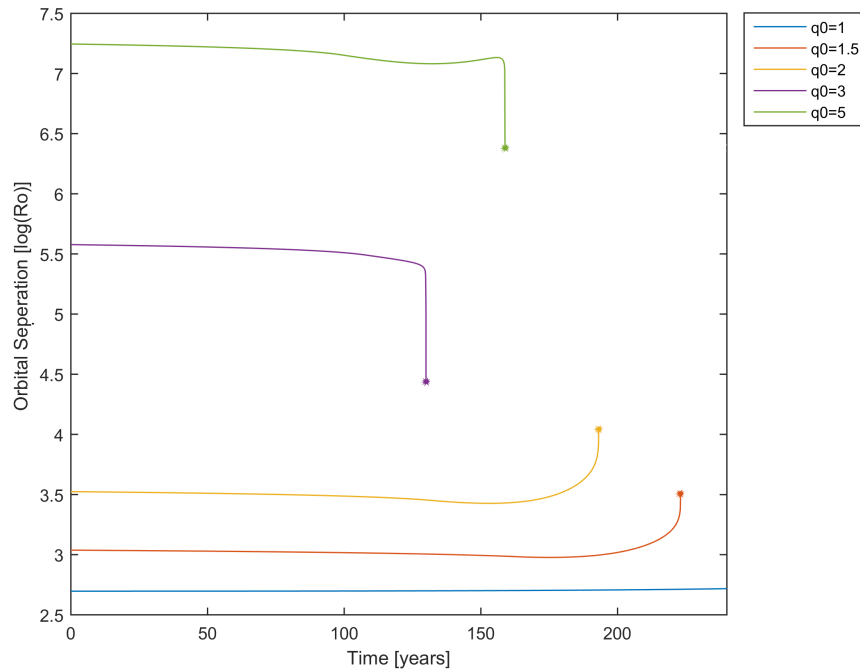


Figure 5.4: Evolution of the logarithmic scaled orbital separation during a non-conservative mass transfer. The big drops seen in the $q_0 = 5, 3$ are caused by mass loss through the outer Lagrange surface. The scale height is set to $\kappa = 0.1$.

Table 5.1: Final separation values when applying the alpha formalism at the start of CEE for $\kappa = 0.01$. Bold text represent merger

$q \downarrow m2 \rightarrow$	$0.25 M_{\odot}$	$0.5 M_{\odot}$	$0.75 M_{\odot}$	$1 M_{\odot}$	$1.25 M_{\odot}$
1	0.11 R_{\odot}	0.31 R_{\odot}	0.45 R_{\odot}	0.49 R_{\odot}	0.52 R_{\odot}
1.5	0.19 R_{\odot}	0.42 R_{\odot}	0.48 R_{\odot}	0.59 R_{\odot}	0.81 R_{\odot}
2	0.27 R_{\odot}	0.45 R_{\odot}	0.58 R_{\odot}	0.93 R_{\odot}	4.56 R_{\odot}
2.5	0.33 R_{\odot}	0.49 R_{\odot}	0.80 R_{\odot}	4.43 R_{\odot}	27.0 R_{\odot}
3	0.37 R_{\odot}	0.56 R_{\odot}	2.78 R_{\odot}	23.1 R_{\odot}	85.8 R_{\odot}
3.5	0.39 R_{\odot}	0.68 R_{\odot}	7.41 R_{\odot}	79.2 R_{\odot}	218 R_{\odot}
4	0.39 R_{\odot}	0.87 R_{\odot}	23.5 R_{\odot}	187 R_{\odot}	517 R_{\odot}
4.5	0.40 R_{\odot}	2.90 R_{\odot}	103 R_{\odot}	424 R_{\odot}	1280 R_{\odot}
5	0.42 R_{\odot}	5.77 R_{\odot}	223 R_{\odot}	1050 R_{\odot}	2990 R_{\odot}

Table 5.2: Final separation values when applying the alpha formalism at the start of Roche lobe overflow for $\kappa = 0.01$. Blank spaces represent systems in which the Roche lobe was not reached.

$q \downarrow m2 \rightarrow$	$0.25 M_{\odot}$	$0.5 M_{\odot}$	$0.75 M_{\odot}$	$1 M_{\odot}$	$1.25 M_{\odot}$
1	0.10 R_{\odot}	0.25 R_{\odot}	0.36 R_{\odot}	0.37 R_{\odot}	0.39 R_{\odot}
1.5	0.16 R_{\odot}	0.34 R_{\odot}	0.37 R_{\odot}	0.44 R_{\odot}	0.60 R_{\odot}
2	0.24 R_{\odot}	0.37 R_{\odot}	0.46 R_{\odot}	0.71 R_{\odot}	3.62 R_{\odot}
2.5	0.31 R_{\odot}	0.41 R_{\odot}	0.64 R_{\odot}	3.68 R_{\odot}	23.0 R_{\odot}
3	0.36 R_{\odot}	0.48 R_{\odot}	2.38 R_{\odot}	20.5 R_{\odot}	77.5 R_{\odot}
3.5	0.38 R_{\odot}	0.59 R_{\odot}	6.73 R_{\odot}	74.2 R_{\odot}	210 R_{\odot}
4	0.39 R_{\odot}	0.77 R_{\odot}	22.5 R_{\odot}	185 R_{\odot}	
4.5	0.40 R_{\odot}	2.74 R_{\odot}			
5		5.75 R_{\odot}			

Table 5.3: Final separation values when applying the alpha formalism at the start of CEE for $\kappa = 0.1$. Bold text represent merger and gray text represent system that remained stable.

$q \downarrow m2 \rightarrow$	$0.25 M_{\odot}$	$0.5 M_{\odot}$	$0.75 M_{\odot}$	$1 M_{\odot}$	$1.25 M_{\odot}$
1	4.88 R_{\odot}	16.0 R_{\odot}	28.1 R_{\odot}	36.0 R_{\odot}	44.1 R_{\odot}
1.5	0.47 R_{\odot}	1.10 R_{\odot}	1.16 R_{\odot}	1.40 R_{\odot}	2.01 R_{\odot}
2	0.57 R_{\odot}	0.92 R_{\odot}	1.13 R_{\odot}	1.82 R_{\odot}	18.5 R_{\odot}
2.5	0.66 R_{\odot}	0.88 R_{\odot}	1.40 R_{\odot}	13.6 R_{\odot}	63.4 R_{\odot}
3	0.67 R_{\odot}	0.68 R_{\odot}	0.87 R_{\odot}	3.03 R_{\odot}	7.2 R_{\odot}
3.5	0.12 R_{\odot}	0.20 R_{\odot}	1.65 R_{\odot}	5.72 R_{\odot}	13.8 R_{\odot}
4	0.13 R_{\odot}	0.27 R_{\odot}	3.23 R_{\odot}	10.6 R_{\odot}	24.7 R_{\odot}
4.5	0.13 R_{\odot}	0.91 R_{\odot}	5.88 R_{\odot}	18.7 R_{\odot}	42.9 R_{\odot}
5	0.14 R_{\odot}	1.57 R_{\odot}	10.1 R_{\odot}	31.4 R_{\odot}	69.8 R_{\odot}

Table 5.4: Final separation values when applying the alpha formalism at the start of Roche lobe overflow for $\kappa = 0.1$. Bold text represent merger and gray text represent system that remained stable. Blank spaces represent systems in which the Roche lobe was not reached.

$q \downarrow m2 \rightarrow$	$0.25 M_{\odot}$	$0.5 M_{\odot}$	$0.75 M_{\odot}$	$1 M_{\odot}$	$1.25 M_{\odot}$
1					
1.5					
2					
2.5					
3		0.67 R_{\odot}	1.32 R_{\odot}	4.57 R_{\odot}	10.8 R_{\odot}
3.5	0.19 R_{\odot}	0.31 R_{\odot}	2.53 R_{\odot}	8.71 R_{\odot}	20.85 R_{\odot}
4	0.20 R_{\odot}	0.41 R_{\odot}	4.93 R_{\odot}	16.0 R_{\odot}	37.3 R_{\odot}
4.5	0.21 R_{\odot}	1.40 R_{\odot}	8.95 R_{\odot}	28.1 R_{\odot}	63.6 R_{\odot}
5	0.22 R_{\odot}	2.4 R_{\odot}	15.2 R_{\odot}	46.3 R_{\odot}	101 R_{\odot}

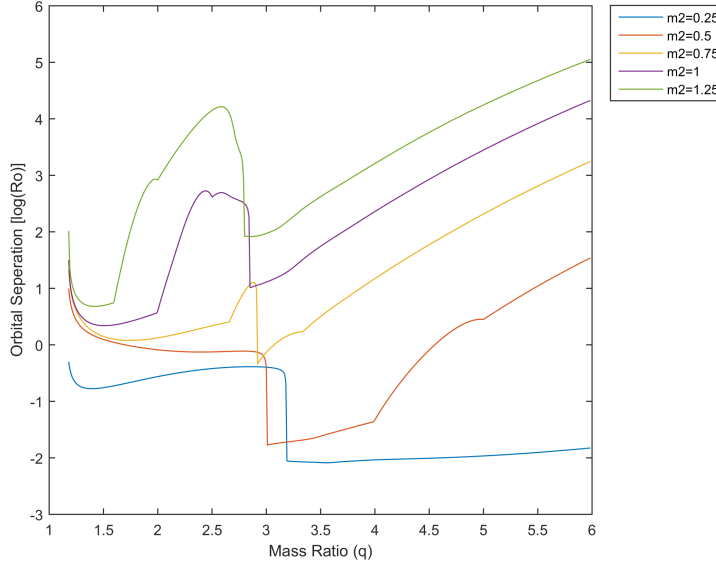


Figure 5.5: Final orbital separation after using the alpha prescription at the start of CEE. κ set to 0.1. Done over a wide range of mass ratio's and with different initial mass on the accretor. The descent from the maximum is due to system's starting their common envelope phase during Roche lobe overflow instead of starting it before.

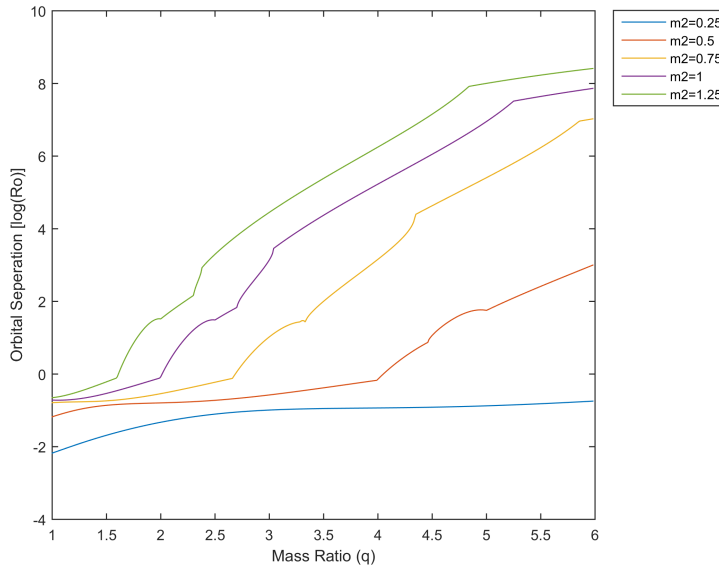


Figure 5.6: Final orbital separation after using the alpha prescription at the start of CEE. κ set to 0.01. Done over a wide range of mass ratios and with different initial mass on the accretor. All the cases except $m_2 = 0.25M_\odot$ follow a linear relationship in general. Different regions of behavior can however still be seen in the lines(explained more in the text). We can see that the mass of the accretor plays a large role in the final separation.

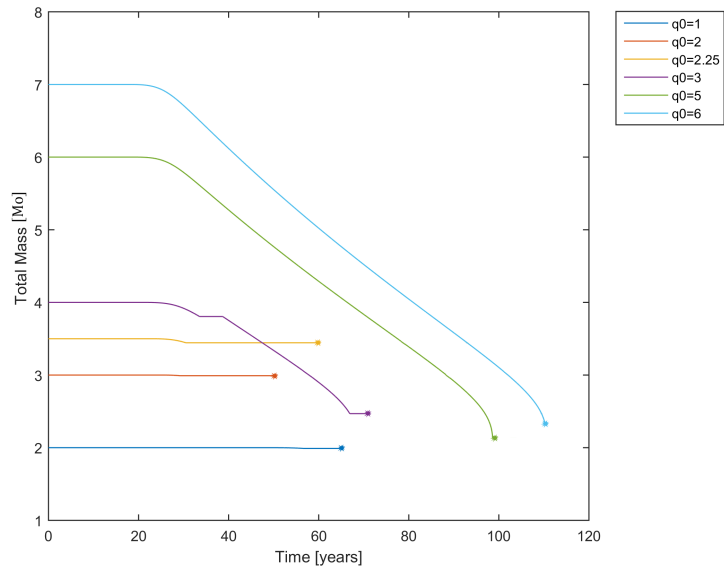


Figure 5.7: Showing the evolution of the mass lost from the system due to mass being blown away by the accretor. The different mass ratio's all belong to different evolutionary regions for the $\kappa = 0.01$ with $m_2 = 1$ case. The $q_0 = 6, 5$ lose almost all of their mass during the plateau phase (see Fig. 5.1). $q_0 = 3$ have two regions in which it loses mass from the system. At about $q_0 = 2.25$ the system enters the plateau phase and start to lose a small amount of mass from the system.

Chapter 6

Summary and conclusions

In this paper we set out to investigate how the onset of common envelope evolution would proceed and to evaluate the importance of different processes. In chapter 3 we went through the stability of mass transfer and concluded that mass transfer from a red giant would in most cases be unstable. This was followed up by showing how a conservative mass transfer would look like with different initial conditions to figure out the effect of different parameters. In chapter 4 we went through the main processes which play a big role in the onset of common envelope evolution. We concluded that significant mass loss from the outer Lagrange point would lead to a collapse in the orbital separation. It was also shown that to build up an envelope the mass transfer rate had to be larger than the Eddington limit and also rapid enough so it would not be blown away by the outward pressure created by the accretor. Lastly we went through the alpha formalism which were used to get the final separation values of the simulations.

From the results we have seen that the nature in which mass transfer proceeds is very sensitive to the scale height of the star κR_* . The scale heights which we choose are a good representation of subgiants ($\kappa = 0.01$) and red giants ($\kappa = 0.1$). This indicates that the time in which a star begins mass transfer during its evolutionary track becomes a very important parameter when considering the final end state of a binary system. We found that subgiants followed a much more predictable behavior in its final separation than that of the red giants. In addition to this we showed that mergers were much more common for subgiant donors than for the red giants. It was shown that the process of mass loss to the outer Lagrange point is significance if the scale height is large enough and that it should play an important role during the mass transfer of more evolved giants. A particular result from this was that we saw that for red giant donors the final separation changed drastically depending on if the common envelope phase occurred before or after its dynamical mass transfer. Another interesting thing that we found was that subgiants which have a lower scale height can experience a stable mass transfer phase before reaching its Roche lobe. As a consequence of this we saw that we could have a widening of the orbit. From the result it also became evident that in both cases the final separation depend strongly on the initial mass of the secondary. If we compare back to our results in the testing section we also saw that the binary of both the red giant and the subgiant case was more stable, becoming unstable at just about $q_0 = 1.18$ and $q_0 = 0.82$ respectively.

In the introduction we also mentioned that we wanted to see if there was any problem in applying the alpha formalism at the onset of Roche lobe overflow. From the results it should be apparent that its application for subgiants and red giants is flawed. First of all in many cases the stars do not even reach the Roche lobe (see table 5.2 and table 5.4). Which we found was due to the fact that we have high amount of mass transfer before Roche lobe overflow. We also saw that in some cases the difference was quite large between applying the alpha formalism at the Roche lobe compared to at the start of CEE. In addition to this, the red giants will have significant mass loss through the outer Lagrange point that the alpha formalism do not take into account.

Acknowledgments

I would like to express my thanks to my supervisor Dr. Ross Church for all his expertise and guidance during the development and writing of this paper.

Bibliography

- Church, R. (2015). Fitting function for the radius of the outer lagrange surface. Private communication.
- de Kool, M. (1990). Common envelope evolution and double cores of planetary nebulae. *ApJ*, 358:189–195.
- Eggleton, P. P. (1983). Approximations to the radii of Roche lobes. *ApJ*, 268:368.
- Eldridge and Tout (20XX). Binary star chapter. In preparation.
- Hurley, J. R., Pols, O. R., and Tout, C. A. (2000). Comprehensive analytic formulae for stellar evolution as a function of mass and metallicity. *MNRAS*, 315:543–569.
- Kolb, U. and Ritter, H. (1990). A comparative study of the evolution of a close binary using a standard and an improved technique for computing mass transfer. *A&A*, 236:385–392.
- Nelemans, G. and Tout, C. A. (2005). Reconstructing the evolution of white dwarf binaries: further evidence for an alternative algorithm for the outcome of the common-envelope phase in close binaries. *MNRAS*, 356:753–764.
- Paczyński, B. (1971). Evolutionary Processes in Close Binary Systems. *ARA&A*, 9:183.
- Passy, J.-C., De Marco, O., Fryer, C. L., Herwig, F., Diehl, S., Oishi, J. S., Mac Low, M.-M., Bryan, G. L., and Rockefeller, G. (2012). Simulating the Common Envelope Phase of a Red Giant Using Smoothed-particle Hydrodynamics and Uniform-grid Codes. *ApJ*, 744:52.
- Pavlovskii, K. and Ivanova, N. (2016). Mass transfer and magnetic braking in Sco X-1. *MNRAS*, 456:263–269.
- Ricker, P. M. and Taam, R. E. (2008). The Interaction of Stellar Objects within a Common Envelope. *ApJ*, 672:L41–L44.
- Ritter, H. (1988). Turning on and off mass transfer in cataclysmic binaries. *A&A*, 202:93–100.
- Rosswog, S. and Brggen, M. (2007). *Introduction to High-Energy Astrophysics*. Cambridge University Press.
- van den Heuvel, E. P. J. (1976). Late Stages of Close Binary Systems. In Eggleton, P., Mitton, S., and Whelan, J., editors, *Structure and Evolution of Close Binary Systems*, volume 73 of *IAU Symposium*, page 35.
- Webbink, R. F. (1984). Double white dwarfs as progenitors of R Coronae Borealis stars and Type I supernovae. *ApJ*, 277:355–360.

Appendix A

Stellar Model

This stellar model is taken from a paper of Hurley et al. (2000). These are the equations used for a star located in the giant branch of its evolution. For simplicity we set the metallicity of the star to $Z = 0.02$. The evolution along the giant branch follow a core mass-luminosity relation that is:

$$L = \min(DM_c^p BM_c^q) \quad (\text{A.1})$$

BM_c^q is introduced to account for the flattening in the relationship when the core mass gets close to the Chandrasekhar mass. DM_c^p however describes the majority of stars. Parameters D,B,q and p are constants in time but will have different values if the initial mass is larger than M_{HeF} . Which is the maximum mass in which helium ignites degenerately in a helium flash.

$$p = \begin{cases} 6 & M \leq M_{HeF} \\ 5 & M \geq 2.5 \end{cases} \quad (\text{A.2})$$

$$q = \begin{cases} 3 & M \leq M_{HeF} \\ 2 & M \geq 2.5 \end{cases} \quad (\text{A.3})$$

$$\log D = \begin{cases} 5.37 [= D_0] & M \leq M_{HeF} \\ \max(-1.0, 0.975D_0 - 0.18M, 0.5D_0 - 0.06M) & M \geq 2.5 \end{cases} \quad (\text{A.4})$$

$$B = \max(3 \times 10^4 .500 + 1.75 \times 10^4 M^{0.6}) \quad (\text{A.5})$$

For cases between M_{HeF} and 2.5 we use linear interpolation of the two cases for continuity. The change in core mass is related to the amount of hydrogen burning in the core which is directly proportional to the luminosity.

$$\dot{M}_c = A_H L \quad (\text{A.6})$$

A_H is the hydrogen rate constant with units $M_\odot L_\odot^{-1} Myr^{-1}$ and depends on the initial mass of the star as:

$$\log A_H = \max[-4.8, \min(-5.7 + 0.8M, -4.1 + 0.14M)] \quad (\text{A.7})$$

If we combine equation A.6 and A.1 we get the following differential equation:

$$\dot{M}_c = A_H DM_c^p \quad (\text{A.8})$$

This equation is used to evolve the core mass in our simulations. The initial value for M_c is given by:

$$M_c = \begin{cases} \begin{cases} [(p-1)A_H D(t_{inf,1} - t)]^{\frac{1}{1-p}} & t \leq t_x \\ [(q-1)A_H B(t_{inf,2} - t)]^{\frac{1}{1-q}} & t > t_x \end{cases} & M < M_{HeF} \\ M_{c,BGB} + (M_{c,Hel} - M_{c,BGB})\tau & M \geq M_{HeF} \end{cases} \quad (\text{A.9})$$

The time spent on the giant branch for stars larger than M_{HeF} is very short and follow a near linear relationship which can be used to approximate the core mass when τ time has passed on the giant branch. For lower mass stars the time is longer and the core follows the relationship given in eq. A.8. t_x in eq. A.9 is the time in which the star enters the high luminosity end of the relationship given in eq. A.1. $\tau, t_x, t_{inf,1}$ and $t_{inf,2}$ is defined as:

$$\tau = \frac{t - t_{BGB}}{t_{Hel} - t_{BGB}} \quad (\text{A.10})$$

$$t_x = t_{inf,1} - (t_{inf,1} - t_{BGB}) \left(\frac{L_{BGB}}{L_x} \right)^{\frac{p-1}{p}} \quad (\text{A.11})$$

$$t_{inf,1} = t_{BGB} + \frac{1}{(p-1)A_H D} \left(\frac{D}{L_{BGB}} \right)^{\frac{p-1}{p}} \quad (\text{A.12})$$

$$t_{inf,2} = t_x + \frac{1}{(q-1)A_H B} \left(\frac{B}{L_x} \right)^{\frac{q-1}{q}} \quad (\text{A.13})$$

The radius of star is modeled as:

$$R_{GB} \approx 1.1M^{-0.3}(L^{0.4} + 0.383L^{0.76}) \quad (\text{A.14})$$

Fig. A.1 show how the radius evolve during dynamical mass transfer for stars with different masses and that are on different points on the giant branch. We can see that we have quite an increase in the radius if we take a star that has evolved half way through its giant branch.

For more information and details we refer to the paper by Hurley et al. (2000)

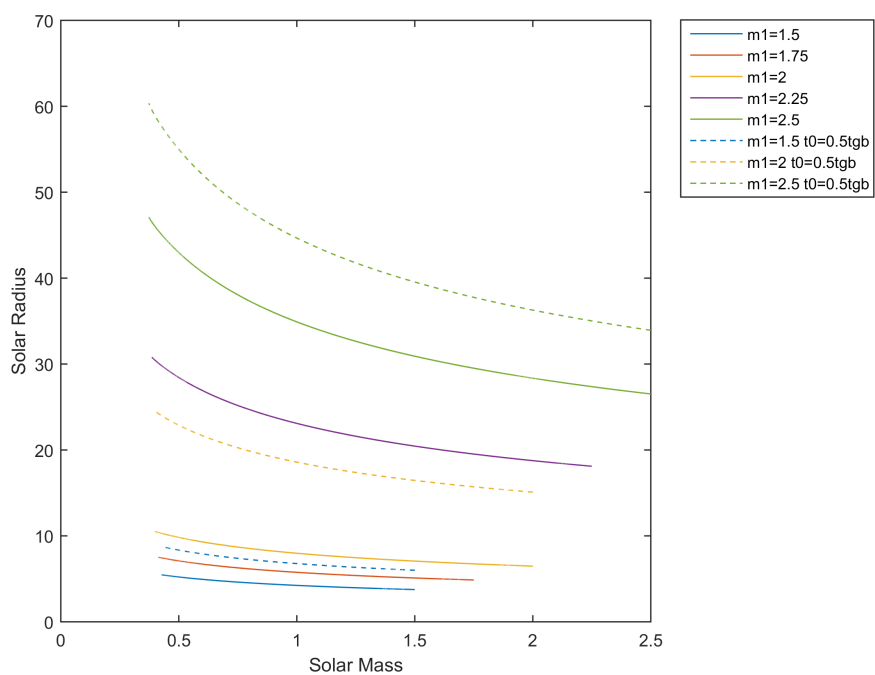


Figure A.1: Shows how the radius of the star changes with mass using different initial masses. The solid line represent systems at the start of their giant branch while the dashed lines represent systems that are half way through their giant branch. Dynamical mass transfer means that we have no change in core mass, which means the curves basically goes as $M^{-0.3}$.